Delamination testing and simulation of hot stamped aluminum alloy/carbon fiber composite laminate

Xinyu Zhang[1], Bin Zhu[1], Tao Li[2,*] and Yisheng Zhang[1]

[1]*State Key Laboratory of Materials Processing and Die & Mould Technology, Huazhong University of Science and Technology, Wuhan 430074, China*

[2]*Dongfeng Motor Corporation Research & Development Institute*

**E-mail: lit@dfmc.com.cn*

The evolution of automobiles necessitates a balance between weight reduction and enhanced safety. Leveraging the hot stamping technique for manufacturing aluminum alloy and carbon fiber-reinforced polymer (CFRP) composites laminate offers significant potential in the automotive sector due to their advantageous qualities of high strength, low density, and cost-effective processing. This study employs hot stamping to integrate aluminum alloy sheets with CFRP prepreg, yielding aluminum alloy/carbon fiber laminated panels. The research investigates the impact of aluminum alloy surface treatment, consolidation dwell time, consolidation pressure during thermal-hot stamping, and CFRP surface modifications on the adhesive bond strength of hybrid aluminum alloy/CFRP components using delamination experiments. By combining an internally cohesive force model based on fracture toughness energy and the Hashin progressive failure criterion, a finite element model is developed to analyze failure modes in multi-material joints during delamination. Findings indicate that noticeable failure in both aluminum alloy and CFRP did not manifest during delamination. Instead, damage emerged within the resin matrix of k.the bonded area due to tensile stress, accompanied by cohesive damage within the joint. Initial adhesive damage appeared at the boundaries of the bonded region, gradually extending from the periphery towards the central bonding area. The experimental results are verified.

Keywords: Hot stamping; Delamination test; Finite element simulation; Alloy/carbon fiber composite laminate.

1. Research Background

The production of cars requires lightweight materials that are also safe. Hot stamping manufacturing of aluminum alloy/carbon fiber layered composites offers high strength, low density, and low costs, making it a potential fit for the automotive industry. High-strength aluminum and CFRP both offer high specific strength, impact energy absorption, and corrosion resistance. However, CFRP has only about 1-2% elastic strain before failure and poor toughness. By using aluminum as the substrate and reinforced with CFRP, the composite's overall strength can be enhanced while balancing its toughness, and it has a high collision energy absorption capacity.

Current methods for joining aluminum alloy and CFRP involve bonding or mechanical fastening. With bonding, aluminum and CFRP parts are separately produced and then joined using a bonding agent. This process is challenging due to the need for separate manufacturing, ensuring dimensional accuracy, and achieving automated production. Mechanical fastening, like riveting or bolting, offers higher connection strength but adds

Y. Zhang and M. Ma (eds.), *Proceedings of the 7th International Conference on Advanced High Strength Steel and Press Hardening (ICHSU 2024)*, Atlantis Highlights in Materials Science and Technology 3,
https://doi.org/10.2991/978-94-6463-581-2_44

weight and has poor sealing. Therefore, it's proposed to use a warm die to quench high-strength aluminum to a certain temperature, lay CFRP prepreg on the aluminum plate, form a non-cured CFRP-aluminum composite under pressure and temperature, and then perform the aging and curing of the composite parts simultaneously. This approach offers an aluminum alloy-CFRP composite component with excellent overall performance.

Peel testing is essential for studying material joint performance. This study created aluminum alloy-CFRP composite plates. Using the cohesive model, a finite element model was developed to accurately represent these plates. This model was validated through experiments, providing valuable technical knowledge for the production of aluminum alloy/CFRP multi-material composite parts.

2. Experimental process

2.1. *Experimental materials and hot stamping process*

In the experiment, 6061-O aluminum alloy produced by a Chinese company was used, with a plate thickness of 1.5 mm. The CFRP prepreg was produced by a Chinese composite material company, and the mechanical properties of the carbon fiber provided by the supplier are shown in Table 1. The material parameters of the epoxy resin-based carbon fiber prepreg are shown in Table 2.

The process diagram used is shown in Fig.1. The process involves several steps: 1. Surface treatment: cleaned the aluminum alloy with acetone to remove oil and impurities; 2. Heat treatment: heat the aluminum alloy to 550°C for 10 minutes; 3. Quenching: cool the aluminum alloy to improve its properties and control its surface temperature for better CFRP prepreg placement; 4. Connection: lay the CFRP material on top of the aluminum alloy plate and stamp it to connect the two materials; 5. aging and curing: place the formed aluminum alloy/CFRP multi-material plate in a hot blast stove and age the aluminum alloy and cure the epoxy resin simultaneously. The holding temperature is 180°C, and the holding time is 3 hours.

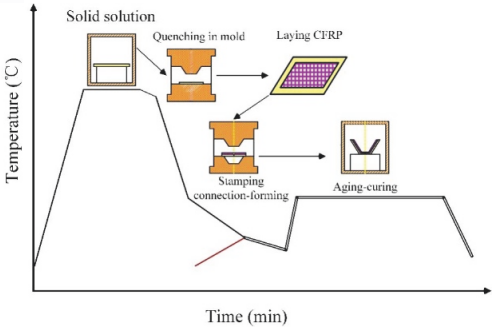

Fig.1 Stamping-bonding process for aluminum alloys and CFRP

Table1 The mechanical properties of the carbon fiber

trademark	Tensile strength /MPa	Elastic modulus /GPa	Linear density /g/Km	Carbon content /%	Diameter /μm
T700	4900	230	800	93	7

Table2 The material parameters of the epoxy resin-based carbon fiber prepreg

Single-layer thickness /mm	Resin content /%	Curing temperature /℃	Curing time /min	Glass transition temperature /℃
0.08	48-60	160-180	180	225-235

2.2. *Peel test process*

The testing standard used was ASTM D1002 in the United States, which determined the shear strength of composite single lap specimens through tension. The size of the peel test specimen is shown in Fig.2, where the individual sizes of the CDRP composite and aluminum alloy plate materials are both 100×25×1.5mm. Fig.3 shows the actual peeled test samples. Before the experiment, ensure that the metal sample surface is dry and clean.

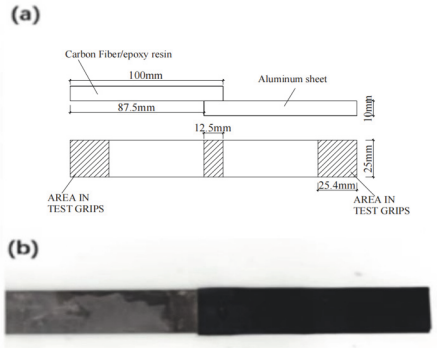

Fig.2 (a) Peel test specimen size; (b) Actual peel test specimens

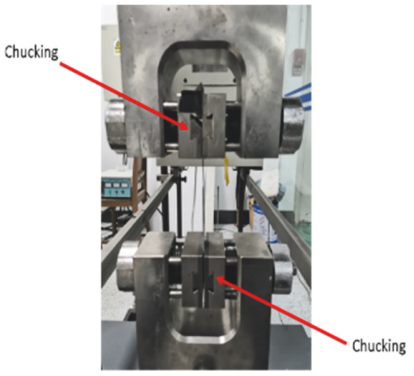

Fig.3 Pictures of the stripping test site

3. Simulation Model

The FEA model of the stripping experiment is shown in Fig.4. The aluminum alloy plate is represented by 3D solid elements C3D8, which are used to create an elastic-plastic model. The CFRP layer is represented using continuous shell elements with fiber orientations of 0°, 90°, 0°, and 90°. When the sum of the squares of the nominal stress ratios in all directions reaches 1, damage begins. The Hashin's progressive damage initiation criterion in ABAQUS and the damage evolution and propagation criteria for CFRP are applied. The calculation of damage evolution is based on fracture energy, and when the energy reaches the initially set maximum value, fracture occurs and the damaged element is allowed to be deleted. The indenter and support are represented using rigid shell elements. The surface friction coefficient is 0.2, allowing limited sliding. The contact is defined as hard contact, ensuring that the discrete rigid body does not deform, with the support completely fixed and limiting all degrees of freedom.

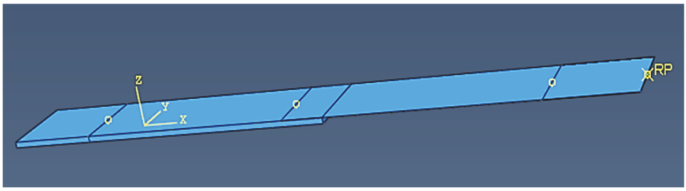

Fig.4 FEA model for peel test

3.1. *Cohesive Zone Model*

The cohesive model represents the force-displacement relationship between two surfaces, including complex material failure and fracture processes. When external loads increase, the crack tip stress increases, and if it reaches the material's limit, damage begins at the aluminum/CFRP interface. As damage occurs, the material's ability to resist external loads decreases, and the interface stress gradually decreases while displacement continues to increase (damage evolution). When the stress decreases to zero, the material interface fails and new cracks propagate. The damage evolution of elements under the cohesion model is calculated based on fracture energy (Gc), and fractures occur when the enclosed area reaches a set value of 1. In this study, the quadratic nominal stress criterion is used as the initial damage criterion in the cohesive zone model. When the sum of the squares of the nominal stress ratios in each direction reaches 1 (as shown in Eq. (1)), damage begins.

$$(\frac{t_n}{t_0})^2+(\frac{t_s}{t_s^0})^2+(\frac{t_t}{t_t^0})^2=1 \tag{1}$$

3.2. *Composite (CFRP) material model*

The failure process of composite materials is a gradual damage process, requiring damage initiation, propagation, and ultimate failure. The Hashin failure criterion is an incremental damage failure model for fiber-reinforced composites in ABAQUS. It includes four failure modes: fiber tensile fracture, fiber compressive fracture, matrix tensile fracture, and matrix compressive fracture. The failure equation is shown in Eq. (2)-(5):

Tensile failure, fiber direction ($\sigma_{11} \geq 0$):

$$F_f^t=(\frac{\sigma_{11}}{X_t})^2+\alpha(\frac{\tau_{11}}{S_l})^2=1.0 \tag{2}$$

Compression failure, fiber direction ($\sigma_{11} < 0$):

$$F_f^c=(\frac{\sigma_{11}}{X_c})^2=1.0 \tag{3}$$

Tensile failure, resin matrix direction ($\sigma_{22} \geq 0$):

$$F_m^t=(\frac{\sigma_{22}}{Y_t})^2+\alpha(\frac{\tau_{12}}{S_t})^2=1.0 \tag{4}$$

Compression failure, resin matrix direction ($\sigma_{22} < 0$):

$$F_m^c = (\frac{\sigma_{22}}{2S_t})^2 + [(\frac{Y_c}{2S_t})^2 - 1]\frac{\sigma_{22}}{Y_c} + (\frac{\tau_{12}}{S_l})^2 \quad (5)$$

In the equations, σ_{11} is the nominal tensile stress in the fiber direction, σ_{22} is the nominal tensile stress in the resin matrix direction, τ_{12} is the nominal shear stress in the fiber direction, $\tau_{12}$is the nominal shear stress in the resin matrix direction, X_t is the longitudinal tensile strength, X_c is the longitudinal compressive strength, Y_t is the transverse tensile strength, Y_c is the transverse compressive strength, S_l is the longitudinal shear strength, S_t is the transverse shear strength, and α is the coefficient for shear stress contribution to fiber tensile initialization criteria.

4. Analysis of results

4.1. *Joint Strength*

During the ABAQUS simulation, the model used two layers of CFRP prepreg with a 0° orientation, matching the rolling direction of the aluminum alloy plate (Fig.5). Fig.6 compares the force-displacement curves from the static peeling experiment and simulation results. In the actual experiment, displacement reached 0.68 mm when the joint strength peaked at 4.3 MPa. As force increased, material failed in steps, causing displacement to gradually decrease. The simulation curve (Fig.6) shows the joint reaching a maximum strength of 4.46 MPa at 0.69 mm displacement, then instantly failing with a drop to 0 strength. Differences in CFRP prepreg performance and resin content caused variations in joint strength between areas, leading to varying failure times in the experiment (Fig.7). These variations were not captured in the finite element model, where consistent material properties caused simultaneous joint failure (Fig.6). The maximum load from experiment and simulation differed by 3.7%, but fracture tough energy measurement confirmed good agreement in mechanical properties and interface adhesion between the experimental and simulated peeling load-displacement curves.

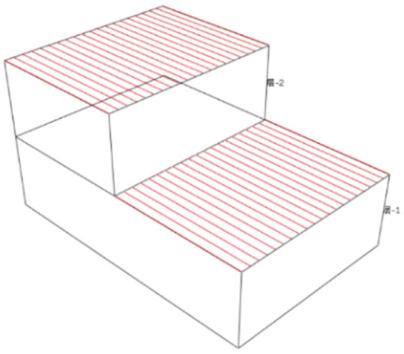

Fig.5 Carbon fiber layup angle

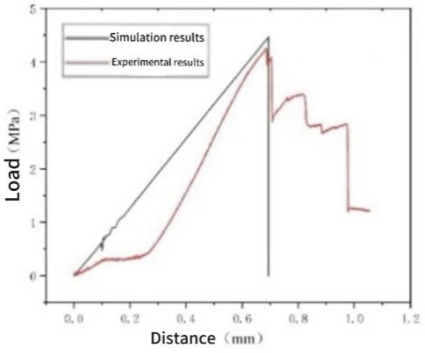

Fig.6 Comparison of the indenter load-displacement simulation curve and the experimental curve of the Al-CFRP specimen

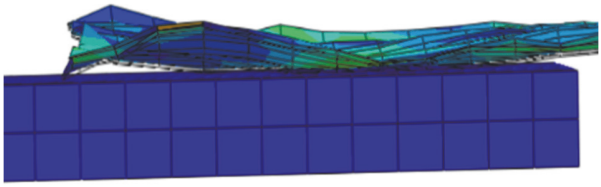

Fig.7 Simulate the specimen topography at failure

4.2. *CFRP Material Damage*

In Fig.8(a), DAMAGEFC shows fiber compression damage. Reaching 1 indicates complete damage evolution and element failure. The figure shows that most of the sample area experiences no compression damage during peeling until failure, aligning with stress conditions. Fig.8(b)'s HSNFCCRT represents fiber compression damage initialization. A value of 1 signifies material satisfying the damage condition and initiating damage evolution. It reveals that at 0.67mm displacement, a small part of the multi-material joint's bond boundary begins to fail. Fig.9(a)'s DAMAGEMT is the fiber tensile damage variable. At 0.68mm displacement, the multi-material joint fails, with only a few elements on CFRP composite boundaries failing. HSNFTCRT is the fiber tensile damage initialization criterion. It starts at 0.67mm displacement, with tensile damage initialization first occurring in the non-bonded aluminum alloy plate area. When the multi-material joint fails, only a few edge elements in the entire fiber region undergo damage; most materials remain intact, indicating that damage evolution in CFRP composite materials occurs after joint failure.

In composite simulations, DAMAGEMC and HSNMCCRT represent matrix compression damage, DAMAGEMT and HSNMTCRT represent tensile damage. CSDMG General_ Contact Domain is a cohesive damage criterion. Fig.10 shows epoxy resin in the matrix doesn't undergo compression damage until the joint fails. Fig.11(b) shows most of the multi-material joint's bonding area starts tensile damage at 0.67mm displacement, peaking at the bonding boundary. Fig.11(a) shows most resin matrix experiences tensile damage, with severity nearer the joint and minimal near the clamp. Fig.12 reveals cohesive damage starts at the bonding boundary at 0.67mm displacement and spreads towards the center as load-displacement increases. The joint's bonding mainly relies on epoxy resin's adhesive properties in CFRP composites. Matrix joint shear strength is lower than carbon fiber, so when the joint fails, carbon fiber doesn't significantly fail, aligning with experimental principles.

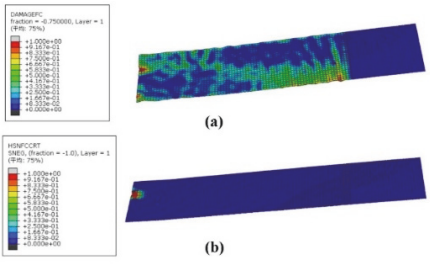

Fig.8 (a) Fiber compression damage variables (The displacement is 0.67mm); (b) Fiber compression initialization (The displacement is 0.67mm)

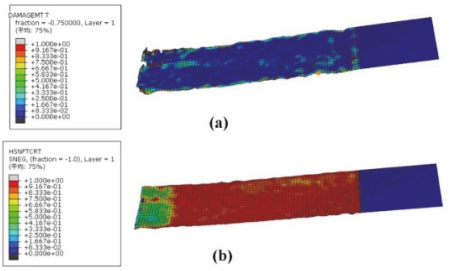

Fig.9 (a) Fiber tensile damage variables (The displacement is 0.68mm); (b) Fiber stretch initialization (The displacement is 0.68mm)

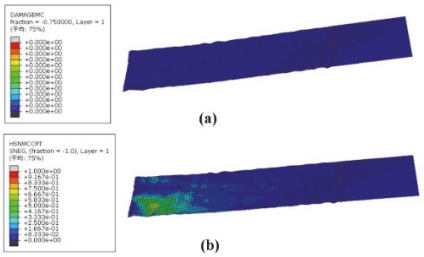

Fig.10 (a) Matrix compression damage variables (The displacement is 0.67mm); (b) Substrate compression initialization (The displacement is 0.67mm)

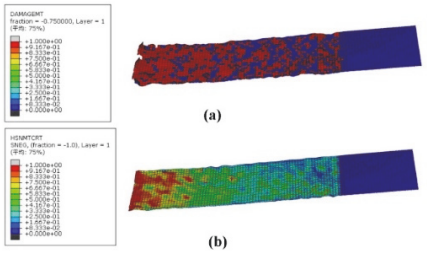

Fig.11 (a) Matrix tensile damage variables (The displacement is 0.68mm); (b) Substrate extrusion initialization (The displacement is 0.67mm)

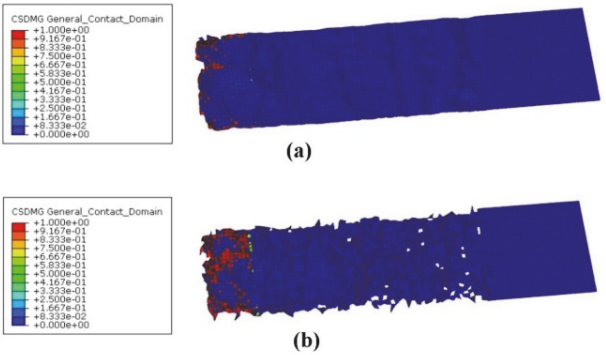

Fig.12 Cohesive damage initialization quadratic nominal stress criterion: (a)The displacement is 0.67mm; (b)The displacement is 0.68mm.

Using finite element simulation for peeling experiments, damage in fiber materials starts at the bonding boundary but doesn't occur until the joint fails. Fiber stiffness reduction is slow until the bonding area fails completely, with no large-scale fiber compression or tension damage. Damage to the resin matrix first appears at the bonding edge of aluminum and carbon fiber plates, then spreads to the bonding area interior until the joint fails. Simulation results show that joint failure mainly takes the form of matrix

tensile damage and cohesive force failure. Damage spreads gradually from the bonding region's boundary to its internal area.

5. Conclusion

The trend of the load-displacement curve is obtained by comparing the experiments, and the finite element simulation curve fails instantaneously at the next shift time when the maximum load is reached, while the experimental curve shows a stepped failure, which is analyzed because the strength of each area of the joint cannot be guaranteed in the experiment, and the properties of each part of the material assisted by finite element modeling are consistent, and each region of the joint fails at the same time.

During the peeling test, when the joint experiences adhesive failure, most areas do not undergo compression damage evolution and only a very small number of edge elements in the fiber region undergo tensile damage evolution. The majority of the material remains intact. When the displacement reaches 0.67 mm, tensile damage occurs in the resin matrix of the bonding area, and cohesive failure occurs in the joint. The adhesive failure first occurs at the boundary of the bonding area and spreads from the boundary towards the center.

References

1. Zhu B, Liu W, Tian F, et al. Research on Hot Stamping-Joining Integrated Process Feasibility of High-strength Steel/CFRP and Sample Bending Performance[J]. China Mechanical Engineering, 2021,32(24):2975.
2. Zhu B, Liu Z, Wang Y, et al. Application of a model for quenching and partitioning in hot stamping of high-strength steel[J]. Metallurgical and Materials Transactions A, 2018,49:1304-1312.
3. Qutaba S, Azhari A, Asmelash M, et al. Development of fiber metal laminate composite with different glass fiber GSM[J]. Materials Today: Proceedings, 2023.
4. Zakeri M, Mansoori H, Sadeghian M, et al. Impact response of fiber metal laminates based on aluminum and UHMWPE composite: Numerical simulation[J]. Thin-Walled Structures, 2022,172:108796.
5. Ghiotti A, Bruschi S, Kain M, et al. Simultaneous bonding and forming of Mg fibre metal laminates at high temperature[J]. Journal of Manufacturing Processes, 2021,72:105-114.